Materials Research Proceedings 41 (2024) 1363-1372 https://doi.org/10.21741/9781644903131-151

Thermomechanical reverse flow forming of AISI 304L

ARIAN Bahman[1,a *], HOMBERG Werner[1], KERSTING Lukas[2,b], TRÄCHTLER Ansgar[2], ROZO VASQUEZ Julian[3,c] and WALTHER Frank[3]

[1]Paderborn University, Forming and Machining Technology (LUF), Germany

[2]Fraunhofer Institute for Mechatronic Systems Design (IEM), Germany

[3]TU Dortmund University, Chair of Materials Test Engineering (WPT), Germany

[a]ba@luf.upb.de, [b]lukas.kersting@iem.fraunhofer.de, [c]julian.rozo@tu-dortmund.de

Keywords: Reverse Flow Forming, α'-Martensite, Grading Strategies, Property-Control

Abstract. In manufacturing, property-control ensures efficient part production. However, in reverse flow forming, current practices focus on geometry-control rather than property-control. To address the complexity of the process and tool-machine interaction, process control is crucial for defined component properties. This study focuses on controlling local α'-martensite content in reverse flow forming of seamless AISI 304L steel tubes. Strategies and systems are presented to influence α'-martensite content, creating unique microstructure profiles for 1D- and 2D-Gradings, with tangible component outcomes.

Introduction

Flow forming excels in precision production of rotationally symmetrical parts, but using semi-finished metastable austenitic steel (AISI 304L) poses challenges due to strain-induced α'-martensite formation [1]. Disturbances like eccentricity and batch variations induce arbitrary microstructural profiles, complicating reproducibility [2]. Manufacturing faces heightened demands for materials, tools, and processes driven by customer expectations for reliability, recyclability, crash safety, and lightweight suitability [3, 4]. The main production objective is defect-free components with local property adjustments, facilitated by closed-loop property-control. Funded by DFG, experimental investigations focus on better control of α'-martensite content during reverse flow forming, aiming for reproducible production with imperceptible microstructure profiles. This innovation enables invisible "barcodes" for product labeling, revolutionizing counterfeiting prevention. Developing process strategies for local α'-martensite manipulation while maintaining external dimensions, using actuator and sensory concepts, is crucial. The current research emphasis is on producing invisible 1D- and 2D-Gradings, as shown in Fig. 1, in an innovative combination of axial and angular grading.

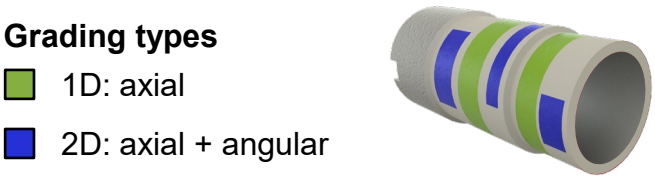

Fig. 1. Differentiation of grading types

Reverse Flow Forming

Flow forming is an incremental process offering various advantages in terms of flexibility and efficiency [5]. A characteristic feature for the process is an intended wall thickness reduction Δw of semi-finished tubes, which leads to component elongation Δl due to volume constancy, accompanied by excellent shape, dimensional accuracy and outstanding surface qualities [6]. Flow formed tubes therefore meet rigorous standards, including those set by the aerospace industry, and are widely used in high-performance components such as drive shafts for jet engines and helicopters [7]. In this paper, the emphasis is on reverse flow forming shown in Fig. 2, a process in which the material flows counter to the axial motion of the roller tools. These roller tools are capable of both radial and axial movement, and they rotate around their own axis due to contact friction with the rotating tube.

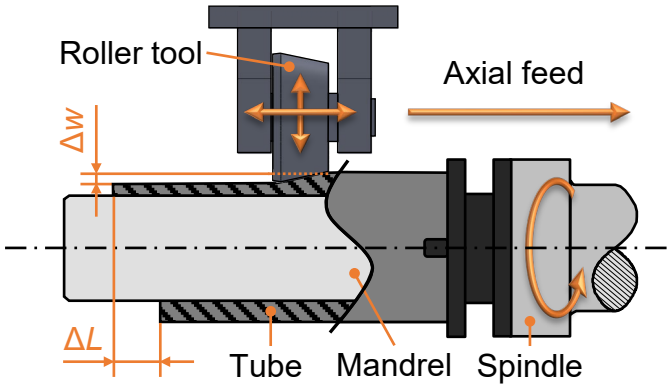

Fig. 2. Reverse flow forming process principle

Experimental Setup

The experiments were carried out on a setup shown in Fig. 3 including a PLB 400 spinning machine from Leifeld Metal Spinning GmbH (Ahlen, Germany) reaching a drive power up to 11 kW and a maximum spindle speed of 950 rpm. The machine is equipped with a hydraulically driven cross support, which has two axes capable of generating a maximum force of 35 kN.

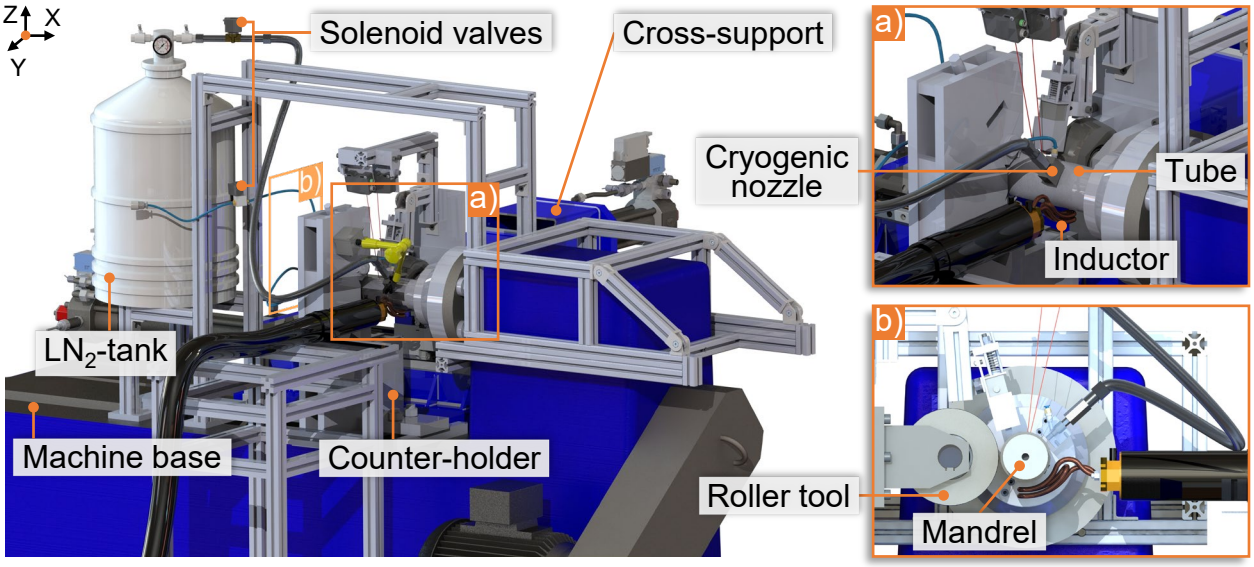

Fig. 3. Machine and actuator configuration with a) and b) showing different viewing angles

The machine setup employs a single-roller tool configuration to accommodate thermal actuator systems and sensors for process control, as outlined in [8]. The sensor concept, developed at Forming and Machining Technology (LUF), will not be the primary focus of this paper. Featuring

a robust counter-holder designed to support the mandrel and an absolute value encoder, the machine can perform angle-dependent operations within the process. The thermal heating actuator consists of a custom-developed inductor that conforms to the shape of the semi-finished tube and can heat a local angular area. The automated cryogenic cooling system, detailed in [9] and illustrated in Fig. 4, serves as a thermal actuator for localized cooling. It enables computer-assisted and reproducible cooling in both axial and/or angular directions. The cryogenic nozzle focuses a -196 °C stream of liquid nitrogen, simultaneously averting the Leidenfrost phenomenon [10].

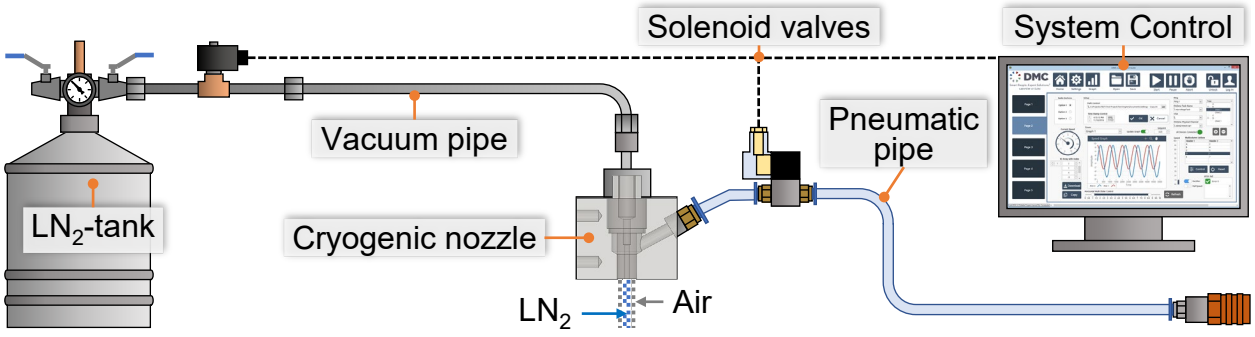

Fig. 4. Automated cryogenic cooling system

The material for the semi-finished tubes is AISI 304L (X2CrNi18-9), a TRIP steel with strain- and/or temperature-induced α'-martensite formation [11]. Detection methods include offline tools like Feritscope and online options like the 3MA-II sensor as addressed in [8] and [12]. The potential for α'-martensite varies with chemical composition, emphasizing the need for property-control.

Grading Strategies

The novel grading strategies aim for 1D- and 2D-graded structures with locally adjusted α'-martensite content useful for functional or sensory purposes in high-performance components.

1D-Grading Strategies:

These circumferential gradings (see Fig. 1) can be performed isothermal only using mechanical actuators or thermomechanical by including thermal actuators. Isothermal strategies create 1D-Gradings through deformation, controlled by process parameters like feed rate *f* and infeed *r*. Thermomechanical strategies, as shown in [9], use a cryogenic cooling system to increase α'-martensite locally or an induction heating system to suppress it. The thermal actuators locally temper the tube, creating a ring of either cool or hot temperature during the process (Fig. 5).

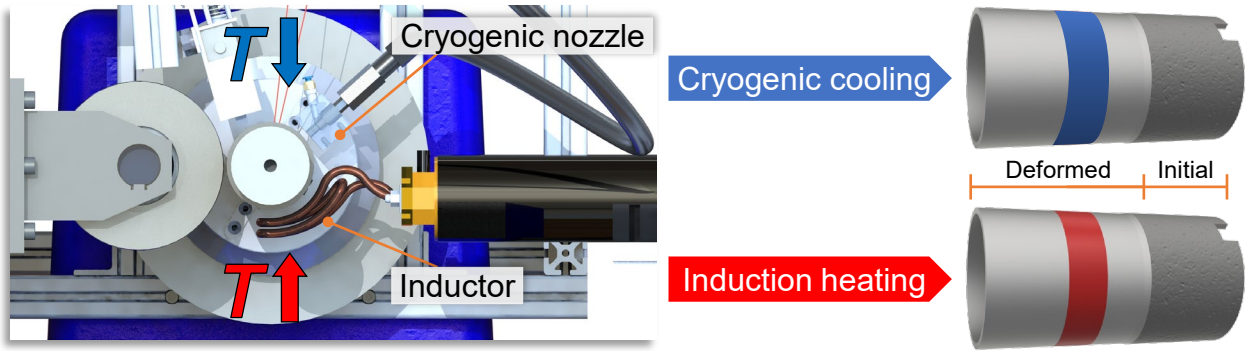

Fig. 5. Thermomechanical strategy for 1D-Grading

2D-Grading Strategies:

For these annular gradings (Fig. 1) isothermal or thermomechanical strategies are possible. Isothermal 2D-Gradings, using an absolute value encoder, involve alternating the radial

positioning of the roller tool to create a visible 2D-Grading on the tube surface (Fig. 6 a) penetration and b) exit process) with a defined grading angle, such as 90° (Stage 1).

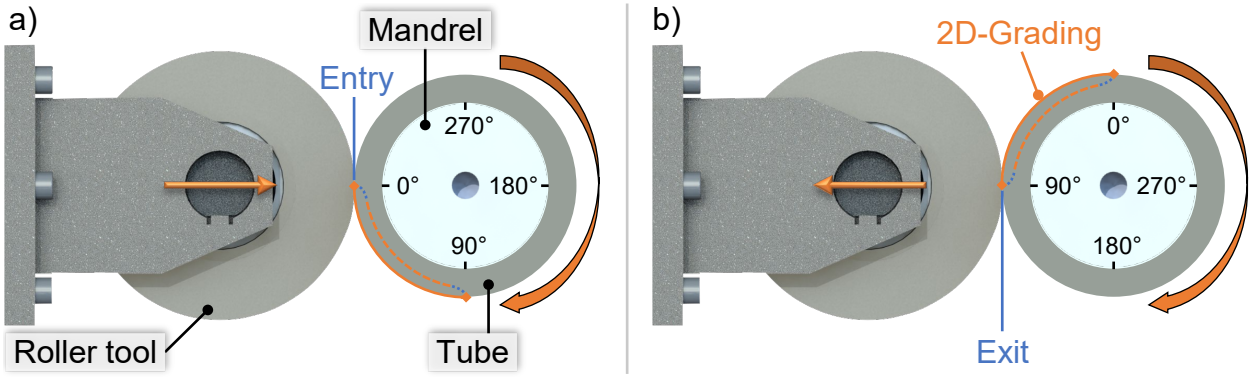

Fig. 6. Mechanical actuator strategy for 2D-Grading with a) penetration and b) exit process

After the initial stage (Stage 1), two strategies can render the 2D-Grading invisible. The first (Stage 2 A) involves turning until the 2D-Grading surface is reached, while the second (Stage 2 B) employs multiple circumferential passes. In contrast, the thermomechanical strategy achieves invisibility in a single stage, using thermal actuators to create an angular temperature gradient. Combining mechanical and thermomechanical strategies is feasible, exploring potential synergies. Liquid nitrogen could enhance α'-martensite formation during 2D-Deformation, while induction heating in the second stage could reduce α'-martensite formation, preventing local resolution loss.

Results and Discussion

Thermomechanical 1D-Grading:

Cryogenic cooling and induction heating (Fig. 5) were employed for 1D-Grading. Cooling/heating the tube surface to approx. -40 °C and 100 °C while forming. Parameters included a 2 mm infeed, 0.1 mm/s feed rate and 30 rpm rotational speed *n*. Both tubes underwent analysis for α'-martensite content and wall thickness. Tempering influenced α'-martensite content without impacting wall thickness. Both exhibited an average 0.68 mm wall thickness reduction over the axial deformation length. Fig. 7 compares α'-martensite distribution, highlighting the differences between cryogenic cooling (Fig. 7 a)) and induction heating (Fig. 7 b)).

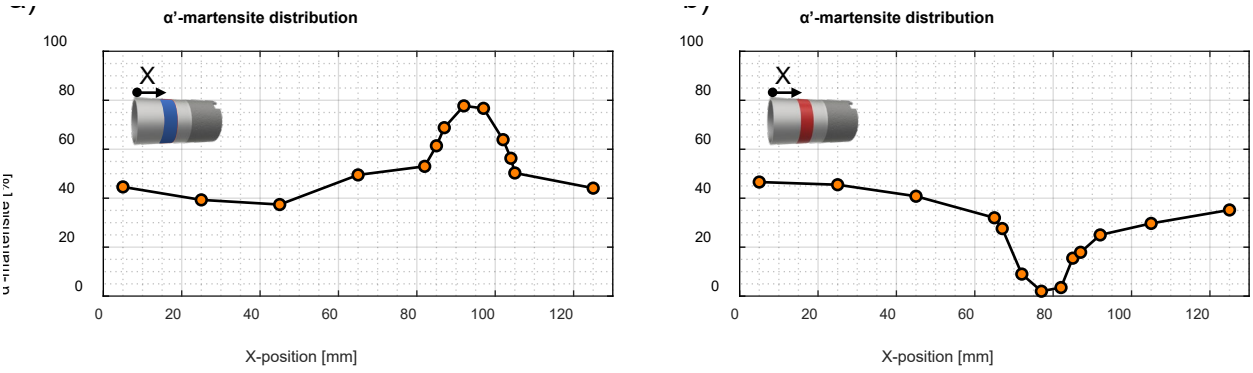

Fig. 7. Thermomechanical 1D-Grading: Distribution of α'-martensite for a) cryogenic cooling and b) induction heating with r = 2 mm, f = 0.1 mm/s, n = 30 rpm and v = $\boldsymbol{f/n}$ = 0.2 mm/rev

Non-tempered areas contained 40% α'-martensite, increased to 80% with cryogenic cooling, and reduced to 1% with induction heating. Tempering of 20 mm in both cases showed thermal actuators achieving a 40% difference in α'-martensite with consistent wall thickness reduction.

Isothermal 2D-Grading:

In Stage 1 a visible 2D-Grading of 90° was performed using 2 mm infeed r, axial feed rate f (X-direction Fig. 3) of 0.1 mm/s, radial feed rate f_r (Y-direction) of 10 mm/s and rotational speed n of 5 rpm (Fig. 8 a)). To enhance surface quality, the axial feed rate was reduced (Fig. 8 b)). The shape of the entry (Fig. 8 c)) and exit region (Fig. 8 d)) result from the geometry of the roller tool and the grading angle of 124.62° (Fig. 8 b)) exceeds the desired 90°, attributed to the exit process.

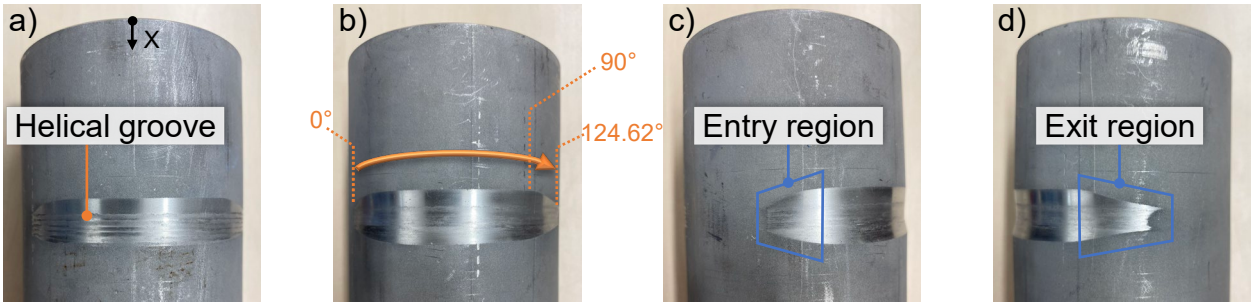

Fig. 8. 2D-Deformation: Using a) suboptimal, b) optimized parameters; c) entry, d) exit region

2D-Deformation measurements included α'-martensite and wall thickness profiles in axial (X-direction) and angular directions (Fig. 9). At the center (30 mm X-position, 180°), both wall thickness reduction (approx. 0.5 mm) and α'-martensite content (approx. 48%) peak (Fig. 9 a)-d)).

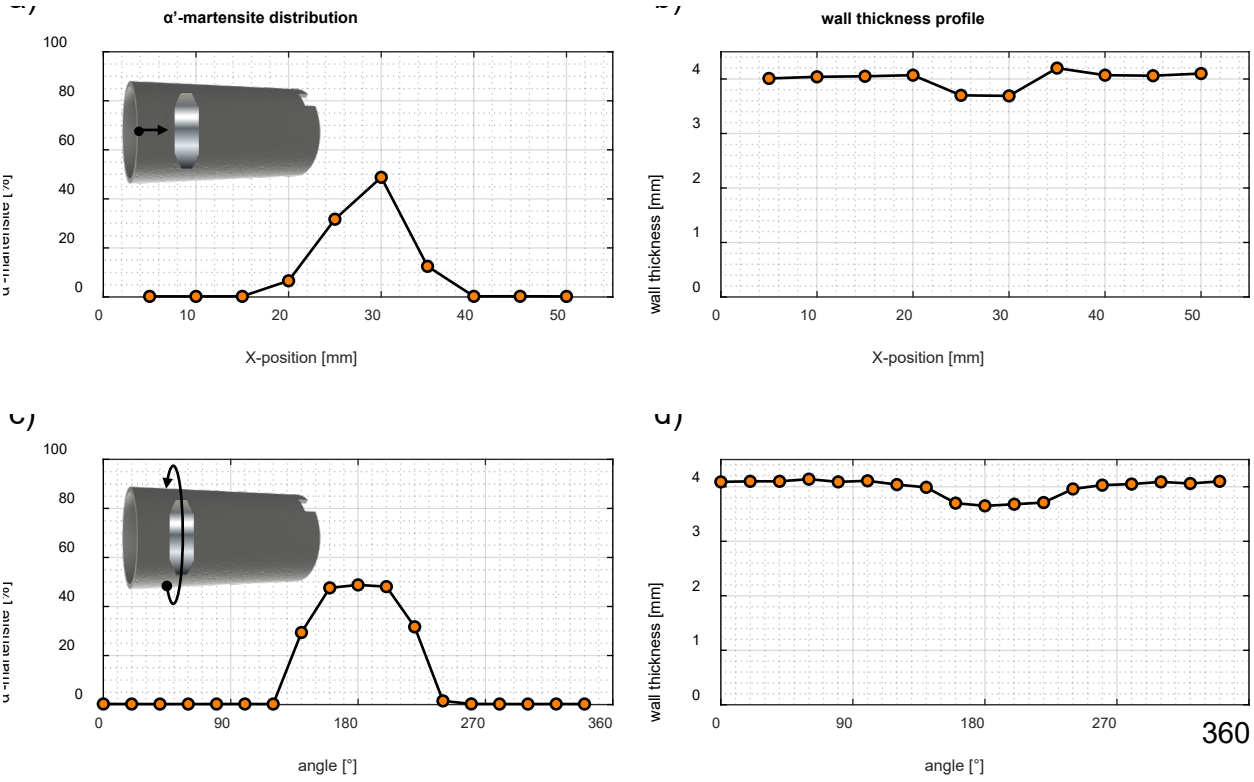

Fig. 9. 2D-Deformation: α'-martensite distribution a) axial, c) angular; wall thickness profile b) axial, d) angular using r = 2 mm, f = 0.017 mm/s, f_r = 10 mm/s, n = 5 rpm and v = 0.2 mm/rev

After the 2D-Deformation in Stage 1, the tube is turned in Stage 2 A (Fig. 10 a)-b)). Post-turning, α'-martensite measurements at various angles (Fig. 10 c)-d)) reveal approx. 0.40% in non-graded areas and 41% in 2D-graded areas. The 2D-Grading is successful and entirely invisible.

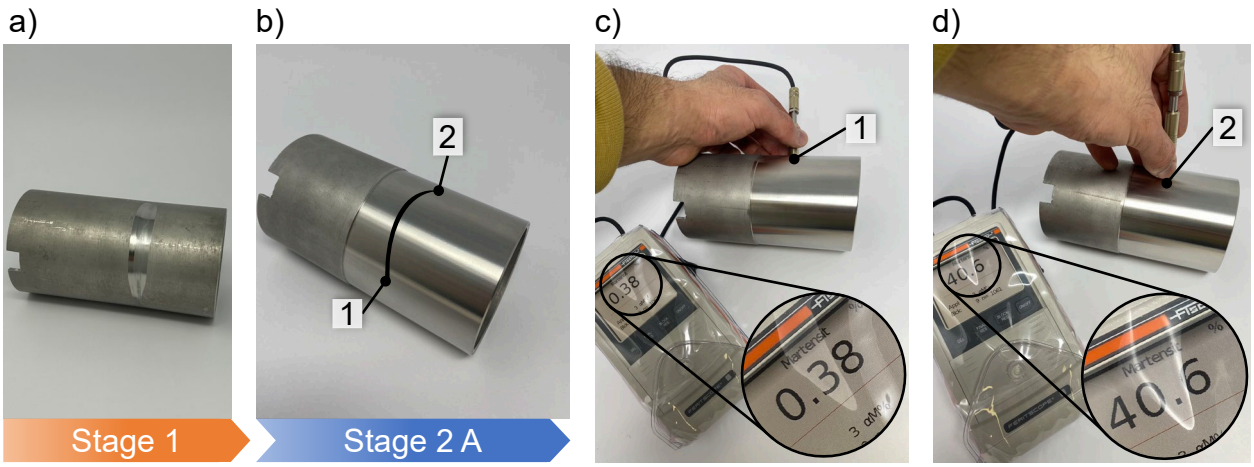

Fig. 10. 2D-Grading: a) 2D-Deformation (Stage 1), b) after turning (Stage 2 A)

An alternative to Stage 2 A is Stage 2 B, using multiple flow forming passes to make the 2D-Deformation invisible (Fig. 11). Fig. 11 a) shows the initial 2D-Deformation, and Fig. 11 b) illustrates the tubes appearance with an increasing number of passes (1-4). Results indicate that an initial 2D-Grading with a 2 mm infeed depth (Stage 1) requires four passes with a 2 mm infeed and a feed speed v of 0.2 mm/rev until becoming invisible. Unlike Stage 2 A, Stage 2 B has no material loss and results in additional tube hardening, providing application-specific advantages.

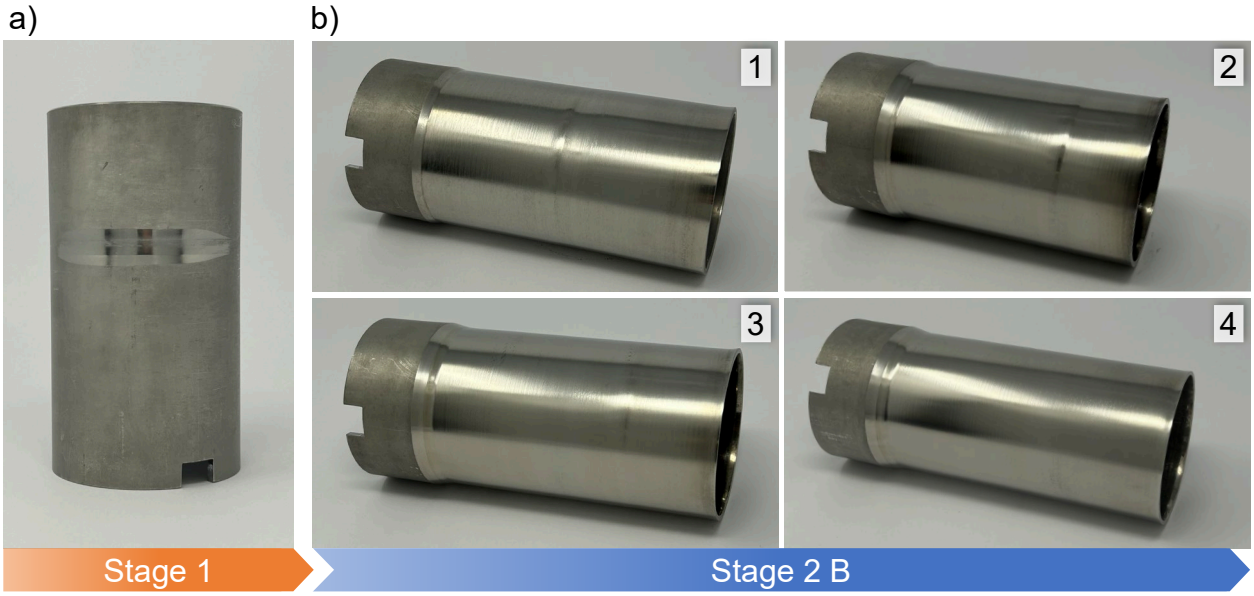

Fig. 11. 2D-Grading: a) 2D-Deformation (Stage 1), b) after multiple consecutive passes 1-4 (Stage 2 B) to make the 2D-Deformation invisible

Fig. 12 depicts α'-martensite distribution and wall thickness profiles in axial and angular directions. The center remains at 30 mm (X-position) and 180° (angle). In Stage 2 B, aiming for 2D-Deformation invisibility, local α'-martensite resolution is compromised. As passes increase starting at approx. 45% α'-martensite content and 0.6 mm wall thickness reduction, curves smooth until similar values at approx. 95% α'-martensite and 2 mm wall thickness reduction emerge.

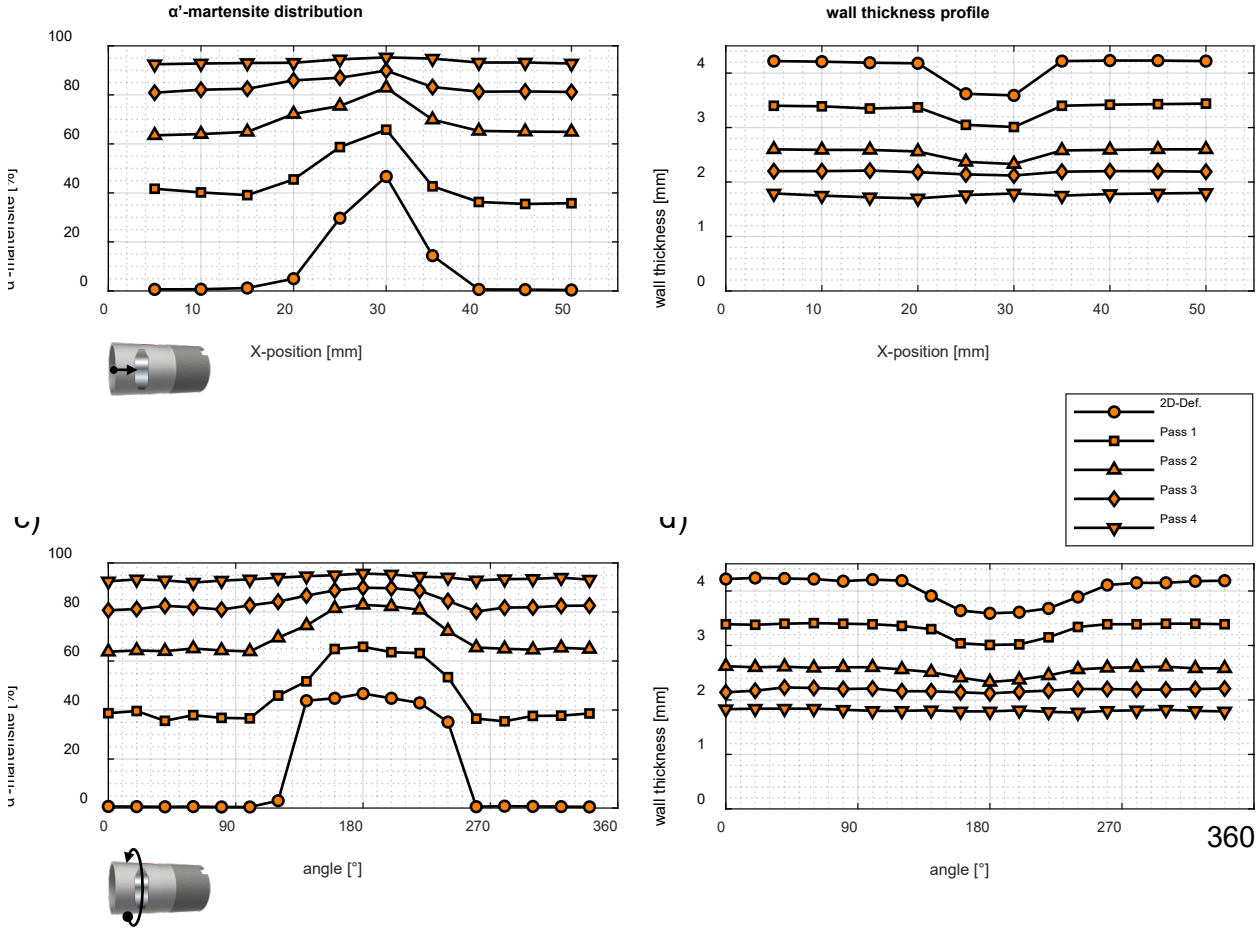

Fig. 12. 2D-Grading: α'-martensite distribution a) axial, c) angular; wall thickness profile b) axial, d) angular for 2D-Deformation (Stage 1) followed by multiple passes (Stage 2 B)

Fig. 13 a) shows the tube produced using the thermomechanical 2D-Grading strategy, employing cryogenic cooling and induction heating systems to create a temperature gradient during tube forming. Measurements in Fig. 13 b) and c) reveal α'-martensite content ranging from about 83% (cooled area) to 2% (heated area) angularly, ensuring uniform wall thickness.

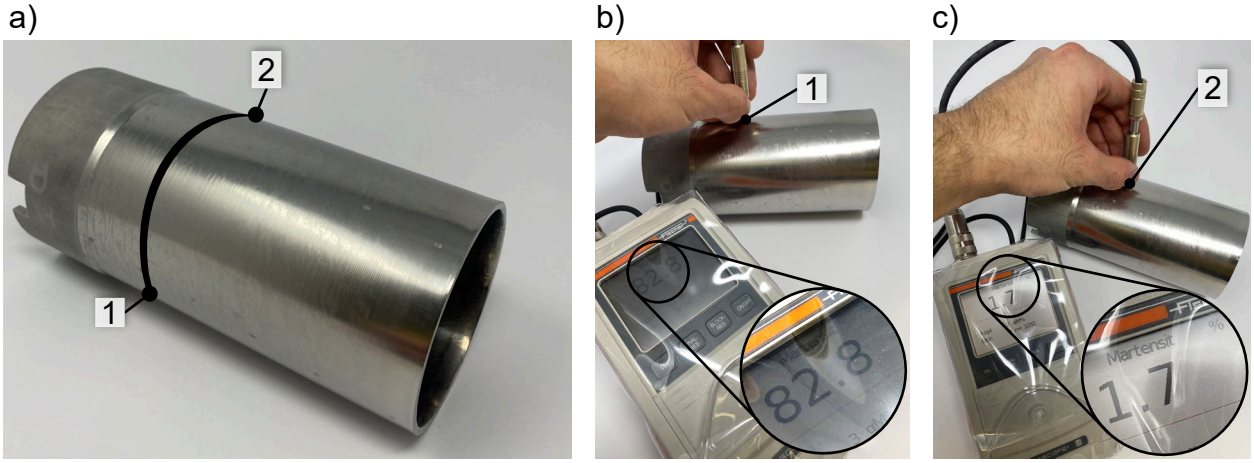

Fig. 13. Thermomechanical 2D-Grading: a) produced tube; b)-c) angular measurement points

Cryogenic cooling cools the tube surface to around -40 °C, while induction heating raises it to about 100 °C to suppress α'-martensite formation. Cooling and heating occur at defined angular regions during rotation, with cryogenic cooling targeting a 90° angular position and induction heating focusing on a 270° position (Fig. 14 b)). Flow forming included a 2 mm infeed, a feed rate of 0.1 mm/s, and a rotational speed *n* of 30 rpm. Wall thickness reduction, approx. 0.65 mm, remained unaffected, resulting in a completely invisible 2D-Grading in this single-stage strategy. In Fig. 14 a), α'-martensite content rises from approx. 45% to 74% until it reaches the center of the heated area at X-position 100 mm, then drops to approx. 2% due to inadvertent cooling of adjacent areas. Successful suppression of α'-martensite formation is shown in an axial range of 20 mm. Fig. 14 b) displays the centers of cooled and heated areas, along with approx. 180° angular ranges where α'-martensite content fluctuates due to cooling and heating effects. The size of these ranges is influenced by factors such as cooling/heating duration, liquid nitrogen flow rate, and induction power. Managing local α'-martensite resolution is complex due to heat conduction.

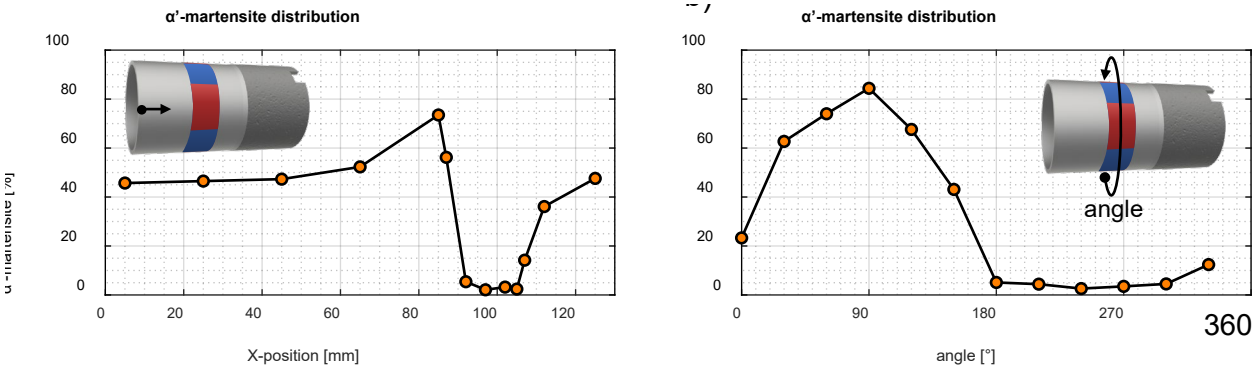

Fig. 14. Thermomechanical 2D-Grading: α'-martensite distribution a) axial and b) angular

Combining the isothermal (Stage 1 and Tage 2 B) and thermomechanical strategies for 2D-Grading offers a solution to address local α'-martensite resolution challenges. The 2D-Deformation takes place (Stage 1) while the area is cooled by the cryogenic cooling system (Fig. 15 a)). In the subsequent stage, the tube exhibiting the visible 2D-Deformation in Fig. 15 b) undergoes multiple passes, heated by the induction heating system, resulting in an invisible 2D-Grading (Fig. 15 c)-d)). Once again, tempering did not affect the wall thickness reduction.

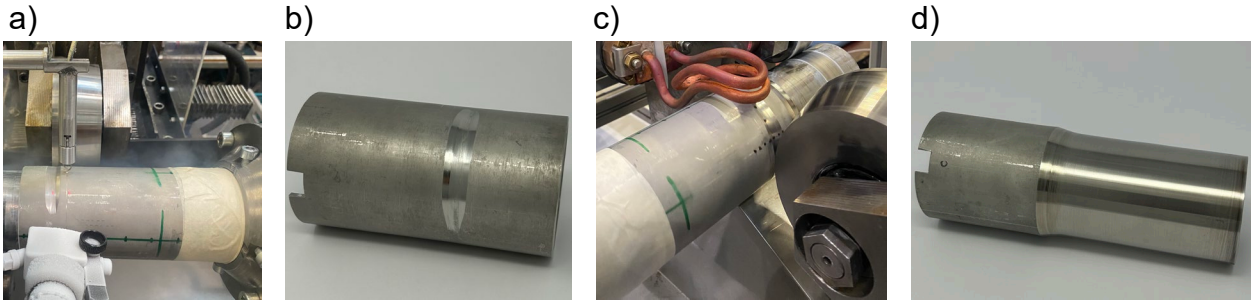

Fig. 15. Combined 2D-Grading strategy: a)-b) cryogenic 2D-Deformation, c)-d) heated passes

Fig. 16 a) and c) show an increase in α'-martensite content compared to the isothermal strategy (Fig. 16 b) and d)). An improvement of the local resolution of α'-martensite content was also visible, without sacrificing resolution through multiple flow forming passes. This approach offers enhanced control over angular α'-martensite distribution, as the resolution is no longer solely dependent on thermal conduction.

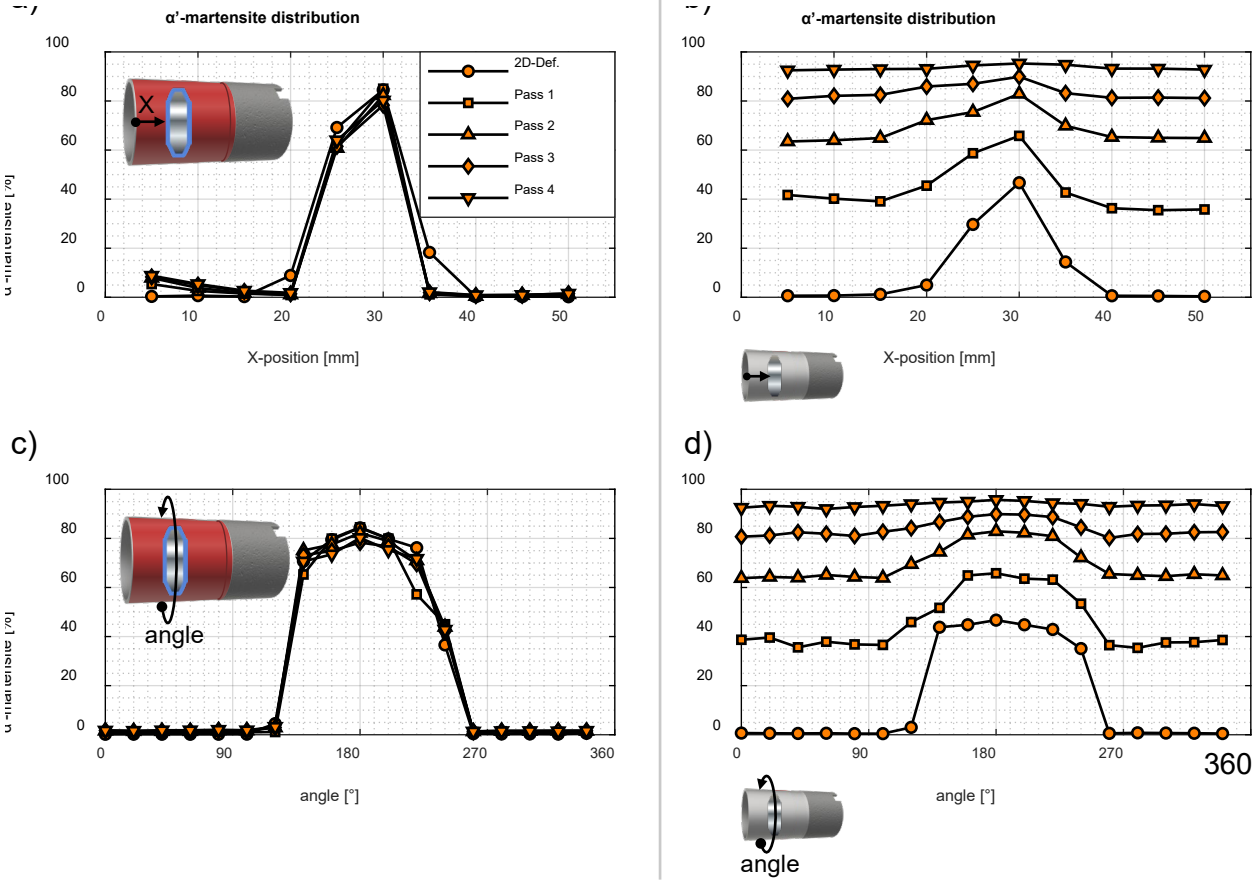

Fig. 16. Comparing α'-martensite distribution a)-b) axial, c)-d) angular with a) and c) showing the combined 2D-Grading strategy, while b) and d) display the isothermal 2D-Grading strategy

Conclusions and Outlook

In conclusion, exploring functionally grade flow forming components with both 1D- (axial) and 2D- (axial and angular) Gradings has provided valuable insights. Various strategies, including isothermal, thermomechanical, and combined approaches, were examined to influence local α'-martensite content and wall thickness profiles. Cryogenic cooling effectively increased α'-martensite content locally, while induction heating efficiently suppressed it. It was shown that these thermal strategies could be applied dynamically and combined for simultaneous cooling and heating, maximizing temperature gradients in locally displaced areas (e.g., to create a ring of hot and cool temperature). Mechanical strategies offer precise adjustment of grading range but may require two-stage designs for invisible 2D-Gradings. Combining isothermal and thermomechanical strategies enhances α'-martensite content significantly while optimizing and ensuring local resolution. Future research aims to advance to 3D-Gradings, influencing α'-martensite content in radial (resp. thickness) direction. These ongoing efforts stand as a testament to the commitment to advancing the understanding and application of functionally graded components in the realm of flow forming.

Acknowledgements

The authors would like to thank the German Research Foundation (Deutsche Forschungsgemeinschaft, DFG) for their support of the depicted research within the priority program SPP 2183 "Property controlled deformation processes", through project no. 424335026 "Property control during spinning of metastable austenites".

References

[1] M. Haridas, G. Gopal, A. Ramesh, R. K. Katta, "Modelling and simulation of single and multi-pass flow forming to investigate the influence of process parameters on part accuracy," *IJMR*, vol. 11, no. 3, 2016, Art. no. 79473. https://doi.org/10.1504/IJMR.2016.079473

[2] M. S. Mohebbi, A. Akbarzadeh, "Experimental study and FEM analysis of redundant strains in flow forming of tubes," *Journal of Materials Processing Technology*, vol. 210, no. 2, pp. 389–395, 2010. https://doi.org/10.1016/j.jmatprotec.2009.09.028

[3] D. Y. Yang *et al.,* "Flexibility in metal forming," *CIRP Annals*, vol. 67, no. 2, pp. 743–765, 2018. https://doi.org/10.1016/j.cirp.2018.05.004

[4] M. Bambach, T. Meurer, W. Homberg, S. Duncan, "Editorial to special issue “Property-controlled forming processes”," *Advances in Industrial and Manufacturing Engineering*, vol. 4, p. 100068, 2022. https://doi.org/10.1016/j.aime.2022.100068

[5] M. Runge, *Spinning and Flow forming: spinning and flow forming technology, product design, equipment, control systems*. Landsberg/Lech: Moderne Industrie, 1994.

[6] M. Sivanandini, S. S. Dhami, and B. S. Pabla, "Flow Forming Of Tubes-A Review," *International Journal of Scientific & Engineering Research*, no. 3, 2012, Art. no. 5. [Online]. Available: https://www.ijser.org/researchpaper/Flow-Forming-Of-Tubes-A-Review.pdf

[7] J. Savoie and M. Bissinger, "Case Studies and Applications of Flowforming to Aircraft Engine Component Manufacturing," *KEM*, vol. 344, pp. 443–450, 2007. https://doi.org/10.4028/www.scientific.net/KEM.344.443

[8] B. Arian, *Produktkennzeichnung durch lokal definierte Einstellung von ferromagnetischen Eigenschaften beim Drückwalzen von metastabilen Stahlwerkstoffen: Ideen Form geben: 36. ASK Umformtechnik : 26.-27. Oktober 2022, Eurogress Aachen : Tagungsband,* 1st ed. Aachen: Verlagshaus Mainz GmbH, 2022.

[9] B. Arian and Materials Research Proceedings (Materials Research Forum LLC), Eds., *Cryogenic reverse flow forming of AISI 304L: Material Forming*, 2023, https://doi.org/10.21741/9781644902479-219

[10] Y. Guo *et al.,* "Delayed Leidenfrost Effect of a Cutting Droplet on a Microgrooved Tool Surface," *Langmuir: the ACS journal of surfaces and colloids*, early access. https://doi.org/10.1021/acs.langmuir.3c00592.

[11] M. Jambor, T. Vojtek, P. Pokorný, and M. Šmíd, "Effect of Solution Annealing on Fatigue Crack Propagation in the AISI 304L TRIP Steel," *Materials (Basel, Switzerland)*, early access. https://doi.org/10.3390/ma14061331.

[12] M. Riepold, B. Arian, J. Rozo Vasquez, W. Homberg, F. Walther, and A. Trächtler, "Model approaches for closed-loop property control for flow forming," *Advances in Industrial and Manufacturing Engineering*, vol. 3, p. 100057, 2021. https://doi.org/10.1016/j.aime.2021.100057